J|A|C|S
ARTICLES
Published on Web 06/21/2006

Theoretical Evidence of PtSn Alloy Efficiency for CO Oxidation

Céline Dupont,[†,‡] Yvette Jugnet,[‡] and David Loffreda*[,†]

Contribution from the Laboratoire de Chimie, UMR CNRS 5182, Ecole Normale Supérieure de Lyon, 46 Allée d'Italie, F-69364 Lyon Cedex 07, France, and Institut de Recherches sur la Catalyse, UPR CNRS 5401, 2 Avenue Albert Einstein, F-69626 Villeurbanne Cedex, France

Received February 23, 2006; E-mail: David.Loffreda@ens-lyon.fr

Abstract: The efficiency of PtSn alloy surfaces toward CO oxidation is demonstrated from first-principles theory. Oxidation kinetics based on atomistic density-functional theory calculations shows that the Pt_3Sn surface alloy exhibits a promising catalytic activity for fuel cells. At room temperature, the corresponding rate outstrips the activity of Pt(111) by several orders of magnitude. According to the oxidation pathways, the activation barriers are actually lower on $Pt_3Sn(111)$ and $Pt_3Sn/Pt(111)$ surfaces than on Pt(111). A generalization of Hammer's model is proposed to elucidate the key role of tin on the lowering of the barriers. Among the energy contributions, a correlation is evidenced between the decrease of the barrier and the strengthening of the attractive interaction energy between CO and O moieties. The presence of tin modifies also the symmetry of the transition states which are composed of a CO adsorbate on a Pt near-top position and an atomic O adsorption on an asymmetric mixed PtSn bridge site. Along the reaction pathways, a CO_2 chemisorbed surface intermediate is obtained on all the surfaces. These results are supported by a thorough vibrational analysis including the coupling with the surface phonons which reveals the existence of a stretching frequency between the metal substrate and the CO_2 molecule.

Introduction

Carbon monoxide oxidation on transition metal and oxide catalysts has attracted much interest in recent years. Tremendous efforts have indeed been devoted to the removal of CO molecule from hydrogen gas fuel aiming at an optimal design of fuel cells. Among the most studied catalysts, the supported platinum-based particles have exhibited a notable efficiency for limiting CO poisoning.[1] However, the current major limitations are the level of CO tolerance and the operating temperature. The improvement of the catalytic performance requires an understanding of the reaction mechanism at the atomic scale. Hence, model approaches on well-defined surfaces have been considered to examine CO reactivity in the fields of surface science and electrochemistry.[2] According to first-principles theory, the oxidation mechanism has been elucidated on various monometallic (111) surfaces.[3−7] The Langmuir−Hinshelwood (LH) mechanism between adsorbed CO and atomic oxygen has been commonly retained. For d transition metal catalysts,[6] the activation barrier is high (0.91−1.71 eV) except on Pt(111) (0.79 eV). For sp metals, the barrier is lower (0.32−0.65 eV).[7]

Among the solutions proposed to activate such a catalytic process, the key role of highly disperse gold particles deposited on oxide supports has been mentioned,[8−12] and more generally the specific high activity of metal oxide supports toward CO oxidation compared to pure metals has been demonstrated from density functional theory (DFT).[6] Attempts to increase the activity by alloying platinum with a second metal have also been reported recently. The presence of a second element such as Ru, Sn, or Mo in the anode catalyst, either alloyed or as a co-deposit with platinum has provided a remarkable improvement of CO tolerance.[13−16] In particular, PtSn supported particles have shown a high activity and selectivity toward CO oxidation in a hydrogen rich atmosphere (PROX).[17] At the fuel cell operating temperature (80 °C), the turnover frequency is about 2 orders of magnitude higher on PtSn/C than on the reference catalyst Pt/Al_2O_3. These results are supported by a recent electrochemistry study on well-defined $Pt_3Sn(hkl)$ surfaces.[18,19]

† Laboratoire de Chimie, UMR CNRS 5182.
‡ Institut de Recherches sur la Catalyse, UPR CNRS 5401.

(1) Oh, S. H.; Sinkevitch, R. M. *J. Catal.* **1993**, *142*, 254.
(2) Marković, N. M.; Ross, P. N., Jr. *Surf. Sci. Rep.* **2002**, *45*, 117.
(3) Alavi, A.; Hu, P.; Deutsch, T.; Silvestrelli, P. L.; Hutter, J. *Phys. Rev. Lett.* **1998**, *80*, 3650.
(4) Eichler, A.; Hafner, J. *Phys. Rev. B* **1999**, *59*, 5960.
(5) Eichler, A. *Surf. Sci.* **2002**, *498*, 314.
(6) Gong, X.-Q.; Liu, Z.-P.; Raval, R.; Hu, P. *J. Am. Chem. Soc.* **2004**, *126*, 8.
(7) Kandoi, S.; Gokhale, A. A.; Grabow, L. C.; Dumesic, J. A.; Mavrikakis, M. *Catal. Lett.* **2004**, *93*, 93.
(8) Cameron, D.; Holliday, R.; Thompson, D. *J. Power Sources* **2003**, *118*, 298.
(9) Bond, G.; Thompson, D. *Gold Bull.* **2000**, *33*, 41.
(10) Bond, G.; Thompson, D. *Catal. Rev. Sci. Eng.* **1999**, *41*, 319.
(11) Haruta, M.; Yamada, N.; Kobayashi, T.; Ijima, S. *J. Catal.* **1989**, *115*, 301.
(12) Haruta, M. *CatTech* **2002**, *6*, 102.
(13) Gasteiger, H. A.; Markovic, N.; Ross, P. N.; Cairns, E. J. *J. Phys. Chem.* **1994**, *98*, 617.
(14) Watanabe, M.; Igarashi, H.; Fujino, T. *Electrochemistry* **1999**, *67*, 1194.
(15) Avgouropoulos, G.; Ioannides, T. *Appl. Catal. B Environ.* **2005**, *56*, 77.
(16) Wang, K.; Gasteiger, H. A.; Markovic, N. M.; Ross, P. N. *Electrochim. Acta* **1996**, *41*, 2587.
(17) Schubert, M. M.; Kahlich, M. J.; Feldmeyer, G.; Hüttner, M.; Hackenberg, S.; Gasteiger, H. A.; Behm, R. J. *Phys. Chem. Chem. Phys.* **2001**, *3*, 1123.
(18) Stamenkovic, V.; Arenz, M.; Blizanac, B. B.; Mayrhofer, K. J. J.; Ross, P. N.; Markovic, N. M. *Surf. Sci.* **2005**, *576*, 145.
(19) Stamenkovic, V. R.; Arenz, M.; Lucas, C. A.; Gallagher, M. E.; Ross, P. N.; Markovic, N. M. *J. Am. Chem. Soc.* **2003**, *125*, 2736.

Several theoretical studies based on first-principles theory have been devoted to the modeling of CO chemisorption on PtRu and PtSn bimetallic alloy surfaces and clusters.[20−25] Two assumptions have been suggested to explain the enhanced CO tolerance on bimetallic catalysts, by considering the adsorption properties of CO and OH surface species.[22,23] The first explanation is a bifunctional mechanism. In this case, an efficient catalyst favors CO adsorption on Pt and OH formation on the second metal. On PtRu(111), both Pt and Ru surface sites are competitive for CO adsorbate.[23] In contrast on $Pt_3Sn(111)$, CO adsorption should occur mainly on Pt, while OH should interact preferentially with Sn.[22,23] Hence, the proximity of CO and OH adsorbed species could explain the promoter effect of tin toward CO oxidation on PtSn anode catalysts. More specifically, the presence of tin could promote the water dissociation and CO oxidation simultaneously.[23] The second explanation is the ligand effect. On the alloy surfaces, the second metal weakens the CO adsorption strength, hence limiting CO poisoning.[20,23] However theoretical investigations of CO oxidation pathways on these multimetallic surfaces have to be solved in order to confirm these interesting assumptions.[26] Moreover oxidation kinetics which have been explored on pure Pt, Rh, and Pd(111) and (100) surfaces from DFT calculations,[5] have to be compared cautiously with the first-principles results on bimetallic surfaces in order to check the theoretical activity gain.

Hence, despite previous experimental and theoretical efforts, fundamental questions still hold regarding the mechanism of CO oxidation on alloy surfaces and, in particular, the reactivity of PtSn surfaces. In fact, the promoter role of tin has to be elucidated concerning the coadsorption structures and the oxidation transition states. The geometric, energetic, and vibrational characterizations of the transition states on the PtSn surfaces have never been investigated before. Moreover, kinetics at the atomic scale should be calculated to compare directly the catalytic activities between pure and bimetallic surfaces. At last in theoretical studies, the final state of the reaction pathway (CO_2) is considered either as a desorbed state ($CO_{2(phys)}$), close to physisorption, undeniably weakly bound,[4,5] or more rarely as an adsorbed state ($CO_{2(ads)}$).[3] Since, DFT approaches describe with difficulty long-range interactions, i.e., van der Waals forces, the $CO_{2(ads)}$ surface species on the Pt(111) surface is still controversial. A thorough analysis of all the adsorbate molecular vibrations coupled with the surface metallic phonons could at least answer the question regarding the existence of a stretching frequency associated with the molecule−substrate bond.

In the following, we aim at answering these key questions from a first-principles approach. More specifically, we show that on two different PtSn surfaces, CO oxidation is easier than on pure Pt surface. The unique role of tin in the lowering of the reaction barrier is also explained on the basis of an energetic decomposition of the activation energy. Moreover, we report on an elementary mechanism with a surface intermediate state for CO_2. According to our models, CO_2 adopts a strongly bent chemisorbed state at the end of the oxidation process.

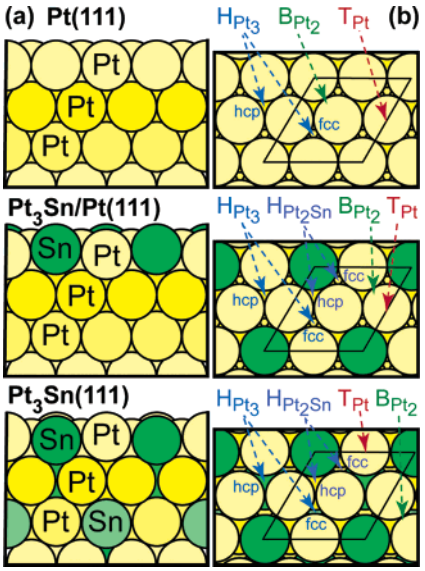

Figure 1. (a) Lateral and (b) top views of Pt(111), Pt_3Sn surface alloy on Pt(111) and $Pt_3Sn(111)$ ((2×2) termination). The competitive sites for isolated CO and atomic O adsorptions are defined in (b) (T, B, and H mean top, bridge, and fcc or hcp hollow site, respectively).

Methodology

The present study is based on density functional theory and periodic metallic slabs. All the results exposed in the following have been obtained with the VASP program.[27,28] Total energy calculations have been performed at the generalized gradient approximation (GGA) with the Perdew−Burke−Ernzerhof (PBE) functional[29] and with the projector-augmented-wave method (PAW).[30] A converged plane-wave cutoff of 400 eV has been considered throughout the study. The supercell approach has been retained for modeling Pt(111), Pt_3Sn deposit on Pt(111), and $Pt_3Sn(111)$ surfaces. The associated coverage chosen here ($^1/_4$ ML) and illustrated in Figure 1 is related to a (2×2) periodicity. To ensure a converged adsorption energy, the Brillouin zone integration has been performed with a $(7 \times 7 \times 1)$ Monkhorst−Pack k-point mesh. The surfaces have been modeled by a periodic slab composed of five metal layers and a vacuum of six equivalent metal layers (14 Å). For the PtSn surface alloy on Pt(111) and the $Pt_3Sn(111)$ surface, the (2×2) termination has been considered, on the basis of previous experimental studies.[31,32] For the surface alloy, a Pt_3Sn monolayer has been deposited on four layers of Pt(111), whereas, for $Pt_3Sn(111)$, each layer has the Pt_3Sn stoechiometry, as depicted in Figure 1. Adsorption occurs only on one side of the metallic slab. The adsorbate and the three uppermost metal layers have been systematically relaxed, while the two lowest metallic planes have been frozen in a bulklike optimal geometry: 2.812 Å for Pt(111), Pt_3Sn/Pt(111) and 2.876 Å for Pt_3Sn-(111).

The minimization of the reaction pathways and the search of the transition states (TS) have been performed with the climbing-image Nudged Elastic Band method (CI-NEB).[33] TS approximate structures are optimized with a set of eight intermediate geometries. The linear interpolation with the Cartesian coordinate system cannot give reason-

(20) Christoffersen, E.; Liu, P.; Ruban, A.; Skiver, H.; Nørskov, J. K. *J. Catal.* **2001**, *199*, 123.
(21) Koper, M. T. M.; Shubina, T. E.; van Santen, R. A. *J. Phys. Chem. B* **2002**, *106*, 686.
(22) Shubina, T. E.; Koper, M. T. M. *Electrochim. Acta* **2002**, *47*, 3621.
(23) Liu, P.; Logadottir, A.; Nørskov, J. K. *Electrochim. Acta* **2003**, *48*, 3731.
(24) Liao, M.-S.; Cabrera, C. R.; Ishikawa, Y. *Surf. Sci.* **2000**, *445*, 267.
(25) Ishikawa, Y.; Liao, M.-S.; Cabrera, C. R. *Surf. Sci.* **2002**, *513*, 98.
(26) Zhang, C. J.; Baxter, R. J.; Hu, P.; Alavi, A.; Lee, M.-H. *J. Chem. Phys.* **2001**, *115*, 5272.
(27) Kresse, G.; Hafner, J. *Phys. Rev. B* **1993**, *47*, 558.
(28) Kresse, G.; Furthmüller, J. *Phys. Rev. B* **1996**, *54*, 11169.
(29) Perdew, J. P.; Burke, K.; Ernzerhof, M. *Phys. Rev. Lett.* **1996**, *77*, 3865.
(30) Kresse, G.; Joubert, D. *Phys. Rev. B* **1999**, *59*, 1758.
(31) Atrei, A.; Bardi, U.; Rovida, G.; Torrini, M.; Zanazzi, E.; Ross, P. N. *Phys. Rev. B* **1992**, *46*, 1649.
(32) Ceelen, W. C. A. N.; van der Gon, A. W. D.; Reijme, M. A.; Brongersma, H. H.; Spolveri, I.; Atrei, A.; Bardi, U. *Surf. Sci.* **1998**, *406*, 264.
(33) Henkelman, G.; Uberuaga, B. P.; Jonsson, H. *J. Chem. Phys.* **2000**, *113*, 9901.

Table 1. Adsorption Energy (eV) of the Main Isolated Adsorption States of Carbon Monoxide (CO) and Atomic Oxygen (O) on Pt(111), Pt_3Sn(111), and Pt_3Sn/Pt(111) Surfaces ($^1/_4$ ML)[a]

	site	Pt(111)	Pt_3Sn(111)	Pt_3Sn/Pt(111)
CO	T_{Pt}	−1.66	−1.50	−1.37
CO	B_{Pt_2}	−1.76	−1.13	−1.41
CO	H_{Pt_3} (Z fcc)	−1.77[b]	−1.14[c]	−1.48[b]
CO	H_{Pt_3} (Z hcp)	−1.78[b]	−1.65[c]	−1.50[b]
O	H_{Pt_3} (Z fcc)	−1.21[b]	−0.14[c]	−0.72[b]
O	H_{Pt_3} (Z hcp)	−0.78[b]	−0.58[c]	−0.54[b]
O	H_{Pt_2Sn} (Pt fcc)		−1.10	−0.84
O	H_{Pt_2Sn} (Pt hcp)		−0.63	−0.54

[a] In each case, the reference state is the bare surface plus CO(gas) or the bare surface plus $^1/_2O_2$(gas). The definition of the sites is given in Figure 1. [b] Z means Pt. [c] Z means Sn.

able initial configurations. Thus the sampling of the intermediate images has been performed in a well-chosen internal coordinate system for the adsorbate, to explore correctly the great variations of the main reaction coordinates: C−O distance and O−C−O angle between CO + O coadsorption and CO_2 physisorption. Once an approximate structure is reached with the CI-NEB approach, the refinement of the TS geometry is achieved by the minimization of the residual forces with a DIIS algorithm (quasi-Newton). Each stationary point of the reaction pathway is then characterized with a complete vibrational analysis.

The technique for the vibrational analysis is based on the numerical calculation of the second derivatives of the potential energy surface within the harmonic approach.[34] In the vibrational treatment, the coupling between the molecular vibrations and the surface phonons of the three uppermost relaxed metal layers is included systematically. Hence the surface phonons are calculated at the Γ point of the unit cell. To calculate the force constants accurately, a tight threshold (below 0.01 eV Å^{-1}) has been applied for the minimization of the residual forces during the geometry optimizations of all the stationary points. The diagonalization of the Hessian matrix provides the harmonic frequencies and the harmonic normal modes of the adsorbate vibrations and the surface phonons.

The calculation of the rate constant for CO oxidation (k^{Ox}) follows the transition-state theory with usual approximations:[35]

$$k_T^{Ox} = k_T^0 \exp\left(\frac{-E_{act}^{ZPE}}{kT}\right) = \frac{kT}{h}\frac{Z_{TS}^{2D}}{Z_{O(a)}^{2D} Z_{CO(a)}^{2D}}\frac{Q_{TS}^{vib}}{Q_{IS}^{vib}}\exp\left(\frac{-E_{act}^{ZPE}}{kT}\right) \quad (1)$$

k^0 is the exponential prefactor including the corrections of vibrational partition functions for the initial state Q_{IS}^{vib} and the oxidation transition state Q_{TS}^{vib}. The initial state corresponds to the CO_{ads} + O_{ads} coadsorption state. These partition functions are computed with the harmonic frequencies. The surface phonons are included systematically. The 2D translation partition functions (Z^{2D}) associated with each surface species (O_{ads}, CO_{ads}, and TS) are also considered. Zero-point energy (ZPE) corrections appear in the calculation of the oxidation activation energy (E_{act}^{ZPE}).

Coadsorption and Oxidation Mechanism

The study of the coadsorption states between CO and O is required to investigate the oxidation reaction pathways. Isolated adsorption of CO and O has been considered first in order to reveal the competitive structures. The geometries of the sites are presented in Figure 1, and the corresponding adsorption energies, in Table 1. On the three surfaces considered here, top adsorption on Pt surface atoms is systematically metastable for

Table 2. Coadsorption Energy (eV) of CO and O on Pt(111), Pt_3Sn(111), and Pt_3Sn/Pt(111) Surfaces ($^1/_2$ ML)[a]

CO_{ads}	O_{ads}	Pt(111)	Pt_3Sn(111)	Pt_3Sn/Pt(111)
T_{Pt}	H_{Pt_3}[b]	−2.76		
T_{Pt}	H_{Pt_2Sn}[b]		−2.50	
H_{Pt_3}[d]	H_{Pt_2Sn}[c]		−1.94	
T_{Pt}	H_{Pt_2Sn}[b]			−2.17
H_{Pt_3}[b]	H_{Pt_2Sn}[b]			−1.83
H_{Pt_3}[c]	H_{Pt_3}[b]			−1.63

[a] Only the states corresponding to stationary points are reported. The reference states are the bare surface plus CO(gas) plus 1/2 O_2(gas). The definitions of the sites are given in Figure 1. [b] Means Pt fcc. [c] Means Pt hcp [d] Means Sn hcp.

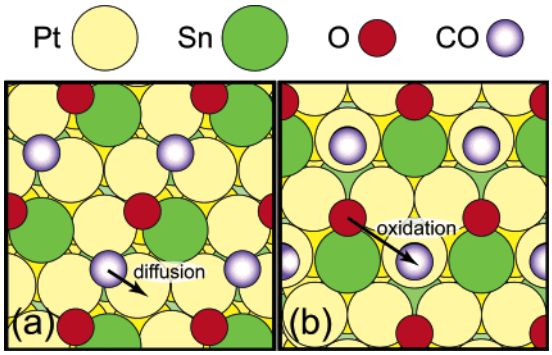

Figure 2. Top views of the competitive CO and O coadsorption structures on Pt_3Sn(111): (a) the metastable structure composed of hollow CO (H_{Pt_3} (Sn hcp)) and hollow O (H_{Pt_2Sn} (Pt hcp)); (b) the stable structure composed of top CO on Pt and hollow O (H_{Pt_2Sn} (Pt fcc)).

CO adsorption: −1.66 eV on Pt(111), −1.50 eV on Pt_3Sn(111), and −1.37 eV on Pt_3Sn/Pt(111). The Pt_3 three-fold hollow site is always the most stable one: −1.78 eV on Pt(111), −1.65 eV on Pt_3Sn(111), and −1.50 eV on Pt_3Sn/Pt(111). On Pt(111), DFT provides the *wrong* relative order between top and hollow adsorption structures by comparison with low-temperature experimental investigations. This apparent contradiction has been evoked several times in the literature[36,37] and clarified recently with both cluster and slab approaches.[38−42] On PtSn surfaces, CO adsorption on tin is not stable. Our results agree with previous DFT calculations on PtSn surfaces.[22,23] For atomic oxygen, three-fold hollow sites are always preferential. On Pt(111), the fcc hollow site is the most stable one (−1.21 eV). In agreement with Watwe et al.'s study,[43] the most stable site on PtSn surfaces is a mixed Pt_2Sn hollow position: −1.10 eV on Pt_3Sn(111) and −0.84 eV on Pt_3Sn/Pt(111).

Once the competitive sites have been determined, coadsorption between CO and O has been considered. The corresponding DFT results have been summarized in Table 2, and the relevant coadsorption states for the oxidation pathways have been presented in Figures 2 and 3 (**5**−**7**). At the considered total coverage ($^1/_2$ ML), the only stable coadsorption structure on Pt(111) is composed of top CO_{ads} and three-fold hollow O_{ads}

(34) Loffreda, D.; Jugnet, Y.; Delbecq, F.; Bertolini, J. C.; Sautet, P. *J. Phys. Chem. B* **2004**, *108*, 9085.
(35) Bocquet, M.-L.; Loffreda, D. *J. Am. Chem. Soc.* **2005**, *127*, 17207.
(36) Feibelman, P. J.; Hammer, B.; Nørskov, J. K.; Wagner, F.; Scheffler, M.; Stumpf, R.; Watwe, R.; Dumesic, J. *J. Phys. Chem. B* **2001**, *105*, 4018.
(37) Grinberg, I.; Yourdshahyan, Y.; Rappe, A. M. *J. Chem. Phys.* **2002**, *117*, 2264.
(38) Geschke, D.; Bastug, T.; Jacob, T.; Fritzsche, S.; Sepp, W.-D.; Fricke, B.; Varga, S.; Anton, J. *Phys. Rev. B* **2001**, *64*, 235411.
(39) Kresse, G.; Gil, A.; Sautet, P. *Phys. Rev. B* **2003**, *68*, 073401.
(40) Gil, A.; Clotet, A.; Ricart, J. M.; Kresse, G.; García-Hernández, M.; Rösch, N.; Sautet, P. *Surf. Sci.* **2003**, *530*, 71.
(41) Mason, S. E.; Grinberg, I.; Rappe, A. M. *Phys. Rev. B* **2004**, *69*, 161401.
(42) Doll, K. *Surf. Sci.* **2004**, *573*, 464.
(43) Watwe, R. M.; Cortright, R. D.; Mavrikakis, M.; Nørskov, J. K.; Dumesic, J. A. *J. Chem. Phys.* **2001**, *114*, 4663.

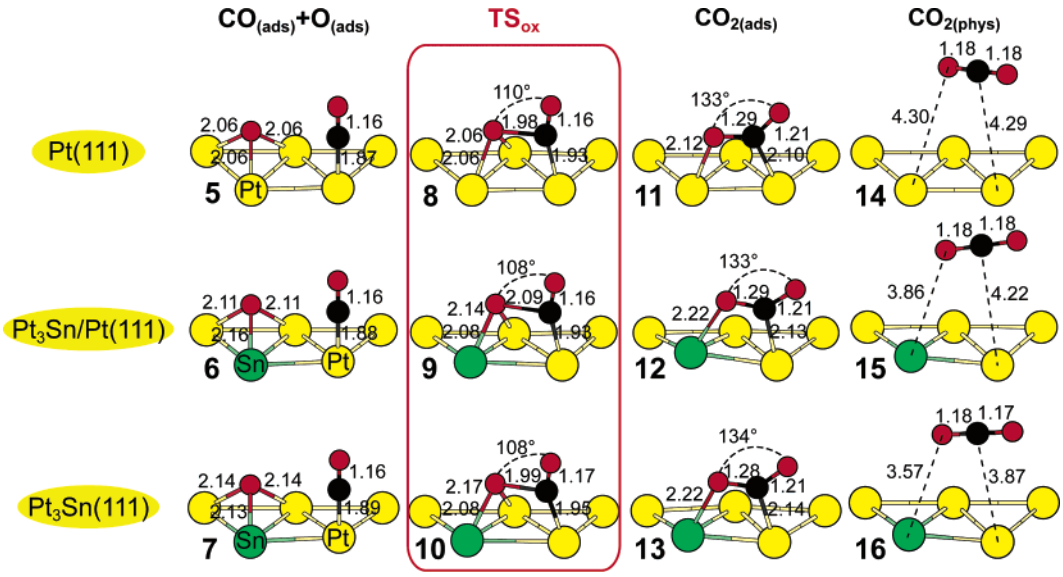

Figure 3. Optimized geometries of the precursor states (coadsorbed CO + O initial states) for CO oxidation (**5**−**7**), the transition states TS_{ox} (**8**−**10**) and the final states (adsorbed $CO_{2(ads)}$ in η_2(CO) structure (**11**−**13**) and physisorbed $CO_{2(phys)}$) (**14**−**16**)). The relevant distances (Å) and angles (°) are reported.

(−2.76 eV). This result agrees with low-energy electron diffraction (LEED) and high-resolution electron energy loss spectroscopy (HREELS) experiments[44,45] at an equivalent coverage (2 × 2) and with previous theoretical results.[26] Hence the increasing coverage and the competition of both reactants in the coadsorption structures induce a change of the most stable site for CO_{ads} from hollow to top. The effect of the coverage on the adsorption energy has already been explained theoretically for CO adsorption on Pd(111) on the basis of a density-of-states analysis.[46] The proximity of both coadsorbates in three-fold hollow positions implies a direct competition for the interaction with the *d* states of the shared Pt surface atom. Such a competition is also observed on PtSn surfaces, as shown in Figure 2. On $Pt_3Sn(111)$, two CO_{ads} + O_{ads} structures compete. For each structure, oxygen is adsorbed on a hollow Pt_2Sn site. In the most stable one (−2.50 eV), CO is coadsorbed on the top Pt site, whereas, in the metastable structure (−1.94 eV), CO is located on the hollow Pt_3 site. Clearly, in the structure reported in Figure 2a with both hollow coadsorbates, CO_{ads} and O_{ads} share the electronic density of Pt surface atoms along the row, whereas, in the most stable structure of Figure 2b, the coadsorbates never interact directly with the same surface metals along the hexagonal pattern. The argument is also valid on the Pt_3Sn/Pt(111) surface, where the most stable coadsorption structure contains CO adsorbed on the top Pt site and O adsorbed on the hollow Pt_2Sn position (−2.17 eV). Among the possible reaction pathways reported for CO oxidation on Pt(111),[4] two different mechanisms have been retained: the bimolecular reaction between coadsorbed CO_{ads} and $O_{2(ads)}$ and the reaction between adsorbed CO and dissociated O. According to Eichler et al.'s results, the CO_{ads} + O_{ads} oxidation route is preferential at high coverage.[4] Since oxidation will be considered at high coverage throughout the study, only the results relative to this second mechanism will be exposed here. A second key point is the choice of the initial coadsorption state for the search of the transition states. As shown before, the most stable coadsorption structures on the three surfaces are always composed of CO adsorbed on the top Pt site and O adsorbed on the hollow site (pure Pt_3 or mixed Pt_2Sn). Hence the corresponding oxidation pathways have all been considered. The oxidation route starting from the metastable state (hollow CO_{ads} and hollow O_{ads}) has also been optimized. However, as it is shown in Figure 2a, this second pathway systematically implies CO diffusion from the hollow to top position prior to oxidation according to the CI-NEB method. Thus only CO top adsorption provides an effective oxidation route (Figure 2b), and the corresponding pathways will be presented in the following section on Pt and PtSn surfaces.

Oxidation Pathways

Before considering the alloy surfaces, the oxidation on the Pt(111) reference surface has been examined in order to validate our approach. The optimized structures, the energy profile, and the calculated barriers are exposed in Figures 3 and 4 and Table 3, respectively. In this work, the metallic surface is precovered by atomic oxygen, and therefore the O_2 dissociation pathway is not presented here. However it has been demonstrated theoretically that the lowest activation barrier is 0.3 eV on Pt-(111).[47] Hence this reaction should not be the rate-determining step of the mechanism, at least on this surface. After O_2 dissociation, the resulting chemisorbed product is atomic oxygen ((**2**), −1.21 eV). CO coadsorption (**5**) allows an energy gain of −1.54 eV, slightly smaller than the CO isolated top adsorption energy (−1.66 eV). Starting from the CO_{ads} + O_{ads} precursor state, the oxygen atom moves toward adsorbed CO resulting in the formation of a C···O bond (1.98 Å) above a hollow site. The transition state (TS_1, **8**) is composed of a bridged oxygen atom and a near-top CO fragment. As shown in Figure 3, the structure is perfectly symmetric with equivalent Pt—O bonds of 2.06 Å. The Pt—C bond is shorter (1.93 Å), whereas the C═O distance is not modified (1.16 Å). The CO_2 angle is slightly open (110°). Our transition state structure agrees with previous calculations on Pt(111).[3,4] More originally, the com-

(44) Kostov, K. L.; Jakob, P.; Menzel, D. *Surf. Sci.* **1997**, *377*−*379*, 802.
(45) Yoshinobu, J.; Kawai, M. *J. Chem. Phys.* **1995**, *103*, 3220.
(46) Loffreda, D.; Simon, D.; Sautet, P. *Surf. Sci.* **1999**, *425*, 68.
(47) Eichler, A.; Hafner, J. *Phys. Rev. Lett.* **1997**, *79*, 4481.

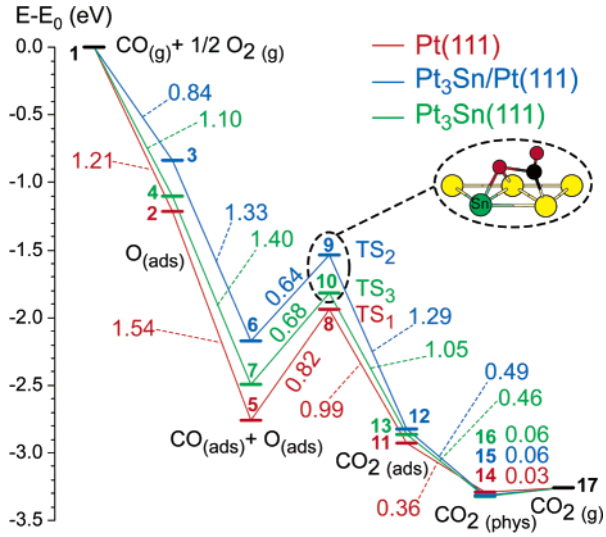

Figure 4. CO oxidation energy profiles (eV) on Pt(111), Pt_3Sn/Pt(111), and Pt_3Sn(111) surfaces. The energy references are clean catalysts and gas-phase CO + $^1/_2O_2$.

Table 3. Oxidation Energy ΔE_{ox} (eV), Oxidation Activation Energy without Zero-Point Energy (ZPE) Corrections E_{act} (eV) and with ZPE Corrections E_{act}^{ZPE} (eV), Preexponential Factor k_{300K}^{0} ($ML^{-1}\ s^{-1}$) and Kinetic Rate Constant k_{300K}^{Ox} ($ML^{-1}\ s^{-1}$) at 300 K for CO Oxidation on the Pt(111) and the PtSn Surfaces

	ΔE_{ox} (eV)	E_{act} (eV)	E_{act}^{ZPE} (eV)	k_{300K}^{0} ($ML^{-1}\ s^{-1}$)	k_{300K}^{Ox} ($ML^{-1}\ s^{-1}$)
TS_1	−0.18	0.82	0.79	3×10^{9}	1×10^{-4}
TS_2	−0.65	0.64	0.61	3×10^{10}	1.5
TS_3	−0.37	0.68	0.67	3×10^{9}	2×10^{-2}

Table 4. Molecular Vibrational Frequencies (cm^{-1}) of the Oxidation Transition States on Pt and PtSn Surfaces (See Figure 5 for the Corresponding Vibrations): a Single Imaginary Frequency ν(C···O), the Stretching Frequency ν(C═O), the Bending Vibration $\delta(CO_2)$ Coupled with the Asymmetric Surface−Molecule Stretching Frequency ν^{as}(M−(O,CO)), the Symmetric Surface−Molecule Stretching Frequency ν^{s}(M−(O,CO)), and Two Frustrated Rotations and Translations, $R_F'(CO)$, $T_F'(O) + R_F''(CO)$, $T_F''(O)$

	Pt(111)	Pt_3Sn(111)	Pt_3Sn/Pt(111)
ν^{im}(C···O)	302i	290i	270i
ν(C═O)	2005	1993	2022
$\delta(CO_2)$, ν^{as}(M−(O,CO))	552	546	531
ν^{s}(M−(O,CO))	446	420	445
R'_F(C═O)	444	459	426
T'_F(O), R''_F(C═O)	335	331	331
T''_F(O)	322	306	301

plete vibrational analysis including the Pt phonons has been performed. The molecular modes are reported in Table 4. A single imaginary frequency ν(C···O) has been found at 302i cm^{-1}. The corresponding vibrational mode is associated with the formation of the C···O bond, as schematized in Figure 5. In agreement with theoretical previous studies,[3−7] the activation barrier is high (0.82 eV). Zero-point energy corrections slightly decrease the barrier (0.79 eV). Our result is consistent with experimental values measured at high coverage on Pt(111) (from 0.50 eV[48] to 0.71 eV[49]) and on Pt/Al_2O_3 (0.79 eV[17]). Once the new C···O bond is formed, the CO_2 molecule remains chemisorbed on the Pt(111) surface in an η_2(CO) position (**11**) according to the CI-NEB approach. This result agrees with Alavi et al.'s study[3] and contrasts with Eichler et al.'s work.[4] The main difference with previous theoretical models is the thickness of the metallic slab. In fact five layers have been considered here, whereas thinner slabs have been optimized before. The $CO_{2(ads)}$ metastable state is a true local minimum on the potential energy surface, according to the vibrational analysis. The Pt−C and Pt−O bonds correspond to chemisorption (2.10−2.12 Å). Both C═O bonds are strongly affected by the adsorption process (1.21 and 1.29 Å). The molecule is particularly bent with a CO_2 angle of 133°. Finally the molecule progressively desorbs; first physisorbed (**14**), then desorbed (**17**). The activation barrier of CO_2 desorption is very small (0.15 eV). As a consequence, CO_2 desorption should occur immediately after the oxidation. The existence of the CO_2 surface species will be discussed later. The physisorbed state (**14**) is associated with an almost gas-phase CO_2 molecule, with equivalent C═O distances of 1.18 Å, lying far above the surface (4.29−4.30 Å).

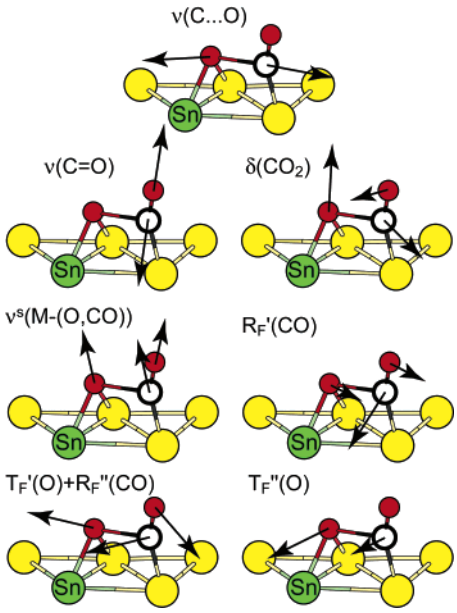

Figure 5. Molecular vibrational modes of the oxidation transition states on Pt and PtSn surfaces: a single imaginary frequency ν(C···O) associated with the formation of the C···O bond, the stretching frequency ν(C═O) of the C═O bond, the bending vibration $\delta(CO_2)$, the surface−molecule stretching frequency ν^{s}(M−(O,CO)), and two frustrated rotations and translations, $R_F'(CO)$, $T_F'(O) + R_F''(CO)$, $T_F''(O)$.

Once having determined the reactivity on the reference surface Pt(111), the particular efficiency of PtSn alloy surfaces for CO oxidation is demonstrated here. On Pt_3Sn(111) and Pt_3Sn/Pt(111) surfaces, the adsorption of atomic oxygen (**3**,**4**) is also destabilized to −1.10 eV on Pt_3Sn(111) and to −0.84 eV on Pt_3Sn/Pt(111), slightly less than that on Pt(111) (−1.21 eV). This large destabilization comes from a direct interaction with a surface Sn atom, as depicted in Figure 3. The precursor states $CO_{ads} + O_{ads}$ (**6**,**7**) are more moderately destabilized from −1.54 eV on Pt(111) to −1.40 eV on Pt_3Sn(111) and −1.33 eV on Pt_3Sn/Pt(111). The stability of the transition states on PtSn surfaces is also decreased. This results in a significant and interesting lowering of the activation barrier: 0.64 and 0.68 eV for Pt_3Sn/Pt(111) and Pt_3Sn(111), respectively. As reported in Table 3, zero-point energy corrections decrease these barriers to 0.61 and 0.67 eV. Our DFT value is higher than the apparent activation energy measured on Pt_3Sn particles supported by carbon (0.32 eV).[17] Rate constant measurements on PtSn sur-

(48) Campbell, C. T.; Ertl, G.; Kuipers, H.; Segner, J. *J. Chem. Phys.* **1980**, *73*, 5862.
(49) Gland, J. L.; Kollin, E. B. *J. Chem. Phys.* **1983**, *78*, 963.

faces are not available in the literature, neither for the bulk alloy truncated surface nor for the deposit. However, an improvement of the catalytic performance has been observed from cyclic voltammetry measurements.[18,50,51] At the transition state (TS_2 for the deposit, **9**, and TS_3 for $Pt_3Sn(111)$, **10**), the formed C···O bonds, 2.09 and 1.99 Å, respectively, are consistently lengthened (cf. Figure 3) and the imaginary frequencies are softer, 270i and 290i cm^{-1}, respectively (see Table 4). The TS geometries are no longer symmetric with shorter O−Sn distances (2.08 Å) due to a buckling of the Sn atom (0.23−0.26 Å). The longer C−O bonds and the more closed CO_2 angles (108°) are clear indicators of an earlier TS on the potential energy surface by comparison with the Pt(111) surface. Such a result is fully compatible with the lowering of the oxidation activation barriers on PtSn surfaces. After the formation of the C−O bond, the molecule remains chemisorbed on the PtSn surfaces, as on Pt(111). Hence a similar elementary mechanism with a metastable intermediate state (CO_2 adsorbed on an η_2−CO−(PtSn) site, (**12**,**13**)) is obtained before desorption (**15**,**16**). The CO_2 adsorption structures correspond to strongly bent geometries on the surface with an open CO_2 angle of 133°−134° and an increased buckling of the Sn atom (0.3−0.4 Å). The Sn−O bonds (2.22 Å) are longer than the ones of the corresponding TS structures. As exposed before on Pt(111), a weak activation barrier is found for CO_2 desorption (0.05 eV). Once the molecule has desorbed, the linear physisorbed states (**15**−**16**) resemble gas-phase CO_2. However they lie closer to the PtSn surface (3.57−4.22 Å) than to Pt(111).

Discussion

DFT oxidation pathways of CO on various Pt and PtSn surfaces have revealed an interesting efficiency of the alloy surfaces and a particular high activity of the deposit Pt_3Sn/Pt(111). The first proof is the lowering of the activation barriers, reported in Table 3. In fact they decrease from 0.79 eV for Pt(111) to 0.61, 0.67 eV for Pt_3Sn/Pt(111), $Pt_3Sn(111)$, respectively. This theoretical indicator is fully consistent with the exothermicity increase of the oxidation step according to the Hammond principle (−0.18 eV for Pt(111), −0.65 and −0.37 eV for Pt_3Sn/Pt(111) and $Pt_3Sn(111)$, respectively). Moreover, the order between the activation barriers is linked to the destabilization of the $CO_{ads} + O_{ads}$ precursor state, in agreement with a previous study devoted to CO oxidation on pure metals and their oxides.[6] To confirm these preliminary results coming from the reaction pathways, the kinetic rate constants of the oxidation elementary step $CO_{ads} + O_{ads} \rightarrow CO_{2(ads)}$ have been systematically calculated, and the corresponding values are presented in Table 3. At 300 K, the oxidation rate constant is relatively weak on Pt(111) (10^{-4} ML^{-1} s^{-1}). The corresponding preexponential factor (3×10^9 ML^{-1} s^{-1}) including vibrational partition functions (see eq 1) agrees with previous experimental kinetic parameters (2×10^{10} ML^{-1} s^{-1}) obtained at high coverage.[48] Previous theoretical calculations without vibrational partition function corrections have provided a larger value (6×10^{12} ML^{-1} s^{-1}).[5] On the $Pt_3Sn(111)$ surface, the reaction rate is 2 orders of magnitude faster at 300 K (2×10^{-2} ML^{-1} s^{-1}), although the absolute value is still relatively weak. Our theoretical result is consistent with experimental observations on a carbon supported bimetallic Pt_3Sn catalyst, where the reaction rate (0.15 s^{-1}) is 2 orders of magnitude faster than that on Pt/Al_2O_3 (2×10^{-3} s^{-1}).[17] More interestingly, the calculated rate constant is 4 orders of magnitude larger on Pt_3Sn/Pt(111) (1.5 ML^{-1} s^{-1}) than on Pt(111). Hence the deposit exhibits an interesting activity at room temperature. Such a result is mainly due to the lowering of the activation barrier but also partially to a larger preexponential factor (3×10^{10} ML^{-1} s^{-1}).

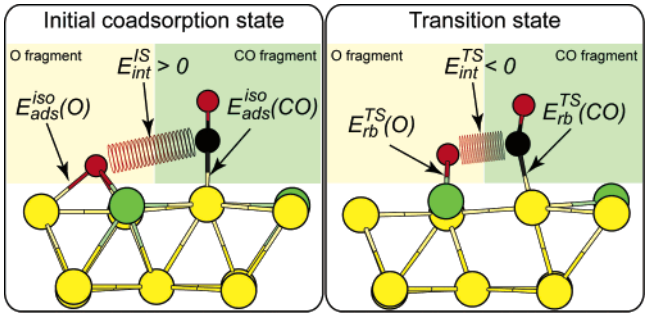

Figure 6. Scheme illustrating the energetic decomposition (CO and O separate fragments) proposed for the initial coadsorption and the transition states (see Table 5).

Table 5. Activation Energy E_{act} (eV), Adsorption Energy E_{ads}^{TS} (eV) of the Transition States on the Three Surfaces and the Corresponding Hammer Analysis: the Rebonding Energy E_{rb}^{TS} (eV) of the CO−Metal Fragment and the O−Metal Fragment in the TS Structure, and the Interaction Energy E_{int}^{TS} (eV) between both CO and O moieties[a]

	Pt(111)	$Pt_3Sn(111)$	Pt_3Sn/Pt(111)
E_{act}	0.82	0.68	0.64
E_{ads}^{TS}	−1.94	−1.81	−1.53
$E_{rb}^{TS}(CO)$	−1.28	−0.94	−0.95
$E_{rb}^{TS}(O)$	−0.49	−0.37	−0.17
E_{int}^{TS}	−0.16	−0.51	−0.41
E_{coads}^{IS}	−2.76	−2.50	−2.17
$E_{ads}^{iso}(CO)$	−1.66	−1.50	−1.37
$E_{ads}^{iso}(O)$	−1.21	−1.10	−0.84
E_{int}^{IS}	0.11	0.10	0.04
$\Delta(\sum E_{frag})$	1.09	1.29	1.09
ΔE_{int}	−0.27	−0.61	−0.45

[a] A similar decomposition is presented for the initial coadsorption states. The variations of the rebonding and the adsorption energy summed over the fragments $\Delta(\sum E_{frag})$ (eV) and of the interaction energy ΔE_{int} (eV) between the initial and the transition states are also reported.

A convenient way to interpret the stability of the transition states has been introduced originally by Hammer for NO dissociation on metal surfaces.[52] In this model, the calculated adsorption energy of the TS (E_{ads}^{TS}) is decomposed into the rebonding energy of CO and O separated fragments in the TS geometry, $E_{rb}^{TS}(CO)$ and $E_{rb}^{TS}(O)$, respectively, and the interaction energy (E_{int}^{TS}) between both CO and O moieties. This decomposition is illustrated in Figure 6, and the results are presented in Table 5. The formulation is derived as follows:

$$E_{ads}^{TS} = E_{rb}^{TS}(CO) + E_{rb}^{TS}(O) + E_{int}^{TS} \qquad (2)$$

The interaction energy is derived by the difference $E_{ads}^{TS} - \sum E_{rb}^{TS}$. A similar decomposition is obtained for the coadsorption

(50) Arenz, M.; Stamenkovic, V.; Blizanac, B. B.; Mayrhofer, K. J. J.; Markovic, N. M.; Ross, P. N. *J. Catal.* **2005**, *232*, 402.
(51) Lee, S. J.; Mukerjee, S.; Ticianelli, E. A.; McBreen, J. *Electrochim. Acta* **1999**, *44*, 3283.
(52) Hammer, B. *Surf. Sci.* **2000**, *459*, 323.

energy of CO and O (E^{IS}_{coads}) at the precursor state with the isolated adsorption energy of CO and O, $E^{iso}_{ads}(CO)$ and $E^{iso}_{ads}(O)$, respectively, and the interaction energy at the initial state (E^{IS}_{int}):

$$E^{IS}_{coads} = E^{iso}_{ads}(CO) + E^{iso}_{ads}(O) + E^{IS}_{int} \quad (3)$$

Hence the activation energy E_{act} is derived easily as a function of the variations of the rebonding and the adsorption energy summed over the fragments $\Delta(\sum E_{frag})$ and the variations of the interaction energy ΔE_{int}, between the initial and the transition states:

$$E_{act} = E^{TS}_{ads} - E^{IS}_{coads} = \Delta(\sum E_{frag}) + \Delta E_{int} \quad (4)$$

Such an expression provides a convenient way to relocalize energetics of the activation barriers on the adsorbate−substrate bonds on one hand and on the CO−O formed bonds on the other hand. According to our DFT calculations, the lowering of the activation barrier between Pt(111) and PtSn surfaces is the result of a simultaneous decrease of the stability of the initial coadsorption states and of the transition states (see Table 5), the former being more destabilized to −2.50 and −2.17 eV, for $Pt_3Sn(111)$ and $Pt_3Sn/Pt(111)$, respectively. Both CO and O moieties exhibit a similar destabilization between pure Pt and PtSn surfaces at the initial states as well as the transition states. This results in a quasi-constant evolution of the variation of the sum of the rebonding energy, from 1.09 to 1.29 eV. This predominant energy term in the calculation of the activation barrier is exactly equivalent between Pt(111) and $Pt_3Sn/Pt(111)$ (1.09 eV). As a consequence, the rebonding energy variation $\Delta(\sum E_{frag})$ does not seem to be intrinsic to a given metallic substrate. In contrast, the second energy term ΔE_{int} in the derivation of E_{act} is stabilizing and is strongly affected by the chemical nature of the surface. This interaction energy variation decreases between Pt(111) (−0.27 eV) and PtSn surfaces (−0.61 and −0.45 eV), hence revealing the stabilizing effect of tin. By comparison with Pt(111), the gain of −0.18 eV for ΔE_{int} in the case of $Pt_3Sn/Pt(111)$ corresponds exactly to the reduction of the barrier. In conclusion, the evolution of the activation energy follows primarily the variation of the interaction energy between CO and O fragments.

The vibrational analysis of the transition state structures supports such an argumentation (cf. Table 4 and Figure 5). In fact, the variations of the molecular vibrations associated with the key reaction coordinates along the potential energy surface (C−O distance, CO_2 angle and the molecule-substrate distances) are correlated with the height of the barrier. More precisely, the lowering of the activation energy between Pt and PtSn surfaces is associated with the weakening of the imaginary frequency (between 302i and 270i cm^{-1}) and the weakening of the $\delta(CO_2)$ bending vibration (from 552 to 531 cm^{-1}). These less energetic vibrations are the signature of a flattening of the potential energy surface on PtSn surfaces and of the existence of earlier transition states. Our assumption is supported also by the lengthening of the C−O distance (from 1.98 to 2.09 Å) and the closing of the CO_2 angle (from 110° to 108°) in the TS structures (see Figure 3).

Finally, the appearance of a surface intermediate in the oxidation mechanism has to be considered cautiously. Although such a surface species has been observed on several metal surfaces,[53] the situation is less clear on Pt(111). The existence of a CO_2 adsorbed state has been proposed previously from experimental measurements on Pt(111)[54] with the technique of Cs^+ reactive ion scattering and on silica supported PtSn alloy[55] but also from theoretical investigations mainly on Ni surfaces[56] and on K-precovered Pt clusters.[57] However, from the theoretical point of view, the existence of such a species is still controversial. Indeed the finding of a metastable CO_2 surface species 0.4 eV above the physisorbed state is worrisome. Moreover, the calculated desorption barrier is very weak on all the surfaces. So the molecule must rapidly desorb at the operating temperature (above 300 K). Hence this hypothetical state cannot be easily detected or checked. A thorough analysis of the adsorbate vibrations on Pt and PtSn surfaces can however improve our understanding of this puzzling state. The molecular frequencies and the corresponding normal modes are exposed in Table 6 and Figure 7, respectively. In fact, even if DFT calculations provide a high stability, the existence of the molecule−substrate

Table 6. Molecular Vibrational Frequencies (cm^{-1}) of the $CO_{2(ads)}$ Surface Intermediate on Pt and PtSn Surfaces (See Figure 6 for the Corresponding Vibrations); the Asymmetric and Symmetric Stretching Frequency, Respectively, $\nu^{as}(CO_2)$ and $\nu^{s}(CO_2)$, of the C=O Bonds, the In-Plane Bending Vibration $\delta(CO_2)$, the Out-of-Plane Wagging Torsional Mode $\omega(CO_2)$, the Surface−Molecule Stretching Frequency $\nu^{s}(M-(C=O))$, and One Frustrated Translation, T_F

	Pt(111)	$Pt_3Sn(111)$	$Pt_3Sn/Pt(111)$
$\nu^{as}(CO_2)$	1762	1757	1748
$\nu^{s}(CO_2)$	1092	1108	1102
$\delta(CO_2)$, $\nu^{as}(M-(C=O))$	676	686	690
$\omega(CO_2)$	552	559	566
$\nu^{s}(M-(C=O))$	331	245	253
T_F	257	287	297

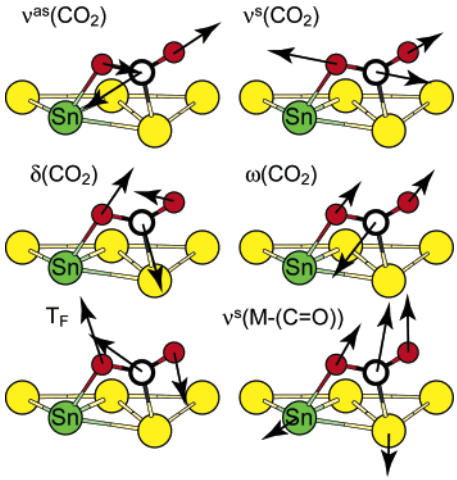

Figure 7. Molecular vibrational modes of the $CO_{2(ads)}$ surface intermediate on Pt and PtSn surfaces; the asymmetric and symmetric stretching frequency, respectively, $\nu^{as}(CO_2)$ and $\nu^{s}(CO_2)$, of the C=O bonds, the in-plane bending vibration $\delta(CO_2)$, the out-of-plane wagging torsional mode $\omega(CO_2)$, the surface−molecule stretching frequency $\nu^{s}(M-(C=O))$, and one frustrated translation, T_F.

(53) Freund, H.-J.; Roberts, M. W. *Surf. Sci. Rep.* **1996**, *25*, 225.
(54) Han, S.-J.; Lee, C.-W.; Yoon, H.; Kang, H. *J. Chem. Phys.* **2002**, *116*, 2684.
(55) Llorca, J.; Homs, N.; Araña, J.; Sales, J.; de la Piscina, P. R. *Appl. Surf. Sci.* **1998**, *134*, 217.
(56) Wang, S.-G.; Cao, D.-B.; Li, Y.-W.; Wang, J.; Jiao, H. *J. Phys. Chem. B* **2005**, *109*, 18956.
(57) Ricart, J. M.; Habas, M.-P.; Clotet, A.; Curulla, D.; Illas, F. *Surf. Sci.* **2000**, *460*, 170.

bond can be solved on the basis of the vibrational analysis including the coupling with the surface metal phonons. According to our results, the asymmetric and symmetric stretching frequencies (respectively, $\nu^{as}(CO_2)$ at 1762 cm^{-1} and $\nu^{s}(CO_2)$ at 1092 cm^{-1}) agree with the observations on Ni(110) or Fe(111) but provide a less good agreement with experiments on K-precovered Pt(111).[53] Moreover, on the three considered Pt and PtSn surfaces, the CO_2—metal bond has been systematically characterized by the existence of substrate−adsorbate low stretching frequency ν^{s}(M—(C═O)) (from 331 to 245 cm^{-1}). As a consequence the present study based on thicker slabs and on the GGA PBE functional supports the mechanism proposed by Han et al. with a CO_2 surface species.[54]

Conclusion

In summary, this study represents a systematic investigation of CO oxidation on Pt and PtSn alloy (111) surfaces from a first-principles approach. On PtSn alloy surfaces, oxidation kinetics based on density functional theory calculations shows a promising increase of the rate constant of 2−4 orders of magnitude by comparison with the Pt(111) surface. The oxidation pathways reveal a significant lowering of the activation energy barrier and an asymmetric structure for the transition states on PtSn surfaces. The promoter effect of tin has been elucidated with an energetic model which links the activation barrier and the variations of the rebonding energy summed over the separate adsorbed reactants and of the interaction energy between CO and O moieties. According to this model, the decrease of the barrier on PtSn surfaces has been correlated with the strengthening of the stabilizing interaction energy. On all the considered surfaces, we report on an elementary mechanism involving a chemisorbed CO_2 surface intermediate. A thorough vibrational analysis including the coupling between the adsorbate vibrations and the metallic surface phonons has demonstrated the existence of a stretching frequency associated with the molecule−substrate bond. According to a previous theoretical study on pure Pt, Cu, and Au(111) surfaces,[7] the H oxidation elementary step (OH formation) competes with the CO oxidation step for the removal of trace amounts of CO. Moreover, in operando conditions, the presence of tin at the anode catalyst should activate the water dissociation and consequently CO oxidation kinetics.[23] Thus, this work supports the assumption that PtSn alloy surfaces should offer an effective activity and selectivity as a PROX catalyst and so a general significance for the fuel cell industry.

Acknowledgment. The authors thank Dr. F. Delbecq (ENS Lyon, France). IDRIS at Orsay is acknowledged for CPU time and assistance (Project 609).

JA061303H